Caveolin-1 Functions as a Scaffolding Protein for Phosphofructokinase in the Metabolic Organization of Vascular Smooth Muscle†

Johana Vallejo and Christopher D. Hardin*

Department of Medical Pharmacology and Physiology, University of Missouri, Columbia, Missouri 65212

Received May 17, 2004; Revised Manuscript Received September 3, 2004

ABSTRACT: Using confocal microscopy, we have demonstrated a similar distribution of phosphofructokinase (PFK) with caveolin-1 (CAV-1) mainly at the periphery (membrane) in freshly isolated vascular smooth muscle (VSM) cells and in cultured A7r5 VSM cells. Co-immunoprecipitation analysis validated the interaction between the proteins. To further test the hypothesis that PFK and CAV-1 are colocalized, we used small interfering RNA (siRNA) to downregulate CAV-1 expression and disrupt the protein−protein interactions between PFK and CAV-1. Transfection of cultured A7r5 cells with CAV-1 siRNA resulted in a decreased level of immunoreactive CAV-1 and a consequent shift in the distribution of PFK with less localization of PFK to the periphery of the cells and increased immunoreactivity at the perinuclear region as compared to control. Analysis of the average PFK intensity across cultured A7r5 cells demonstrated a higher central:peripheral intensity ratio (CPI ratio) in siRNA-treated cells than in the control. These results validate the possible role of CAV-1 as a scaffolding protein for PFK as evidenced by the significant redistribution of PFK after CAV-1 downregulation. We therefore conclude that CAV-1 may function as a scaffolding protein for PFK and that this contributes to the compartmentation of glycolysis from other metabolic pathways in VSM.

Extensive evidence indicates coupling of metabolic cascades to specific processes in different types of cells, and this concept is now emerging as a more general feature of cellular organization. Compartmentation has been described in a wide variety of cells (*1*−*7*). However, the physical basis for the organization and hence compartmentation of cytoplasmic metabolism remains to be fully elucidated. Previous work by our laboratory has shown that a compartmentation of carbohydrate metabolism exists in freshly isolated smooth muscle preparations (*2*−*4*, *8*−*10*) and in cultured rat aorta A7r5 cells (*11*). Using ^{13}C NMR to examine the products of metabolism from glycolysis and gluconeogenesis, we have determined that glycolysis and gluconeogenesis occur in separate compartments within the VSM[1] cell and their respective intermediates do not mix freely within the cytoplasm (*2*−*4*, *8*−*11*). Therefore, spatial separation of glycolytic and gluconeogenenic enzymes and the proximity of the metabolic intermediates to the localized enzymes must be the basis of compartmentation. We have also found that an intact plasma membrane is essential for compartmentation of glycolysis from gluconeogenesis to exist, suggesting that glycolysis and gluconeogenesis may be associated with distinct plasma membrane microdomains (*3*, *4*). Disruption of the specific caveolae plasma membrane microdomains by treatment with cyclodextrin disrupts metabolic flux and compartmentation in VSM cells (*4*). Therefore, we hypothesized that associations of glycolytic enzymes with caveolae membrane domains and gluconeogenic enzymes with noncaveolae membrane domains provide a structural separation of the two metabolic pathways.

Localized glycolytic enzymes may be important in providing metabolic support to nearby ATP-consuming processes. Phosphofructokinase (PFK) is a key enzyme in the control of glycolysis and the regulation of carbohydrate metabolism. It catalyzes the conversion of fructose 6-phosphate to fructose 1,6-bisphosphate which is a unidirectional and rate-limiting step in glycolysis. A number of reports describe the association of PFK with various cytoskeletal elements and with signal transduction proteins, and thus, this localization might underlie the observed compartmentation. In skeletal muscle, PFK associates with tubulin and microtubules under certain conditions (*12*). In cardiac muscle, a fraction of PFK is associated with phospholipase A2 (*13*). Also, insulin stimulates binding of both PFK and aldolase to the cytoskeleton in diaphragm muscle (*14*). In the brain, PFK-M interacts with neuronal nitric oxide synthase (*15*). Recent studies suggest that in differentiated skeletal C2C12 myotubes, PFK associates with caveolin-3 (an integral membrane protein) under certain metabolic conditions (*16*, *17*).

Caveolae are small invaginations 50−100 nm in size in the plasma membrane that have been proposed to provide

† This work was supported by NIH Grant DK60668 (to C.D.H.), NIH Training Grant HL F32-07094 (to J.V.), and a Porter Physiology Fellowship (to J.V.).

* To whom correspondence should be addressed: Department of Medical Pharmacology and Physiology, MA 415 Medical Sciences Building, University of Missouri, Columbia, MO 65212. Telephone: (573) 884-6209. Fax: (573) 884-6209. E-mail: HardinC@missouri.edu.

[1] Abbreviations: AOI, area of interest; CAV-1, caveolin-1; CAV-2, caveolin-2; CAV-3, caveolin-3; CPI ratio, central:peripheral ratio; GAPDH, glyceraldehyde-3-phosphate dehydrogenase; PFK, phosphofructokinase; siRNA, small interference RNA; VSM, vascular smooth muscle.

10.1021/bi0490035 CCC: $27.50
Published on Web 12/03/2004

scaffolding for compartmentalized signal transduction and lipid transport (*18*−*22*). Biochemically, caveolae represent a subdomain of the plasma membrane enriched in cholesterol, glycosphingolipids, and a family of integral membrane proteins named caveolins (*18*, *23*). Three mammalian isoforms of caveolin have been characterized and identified as caveolin-1, caveolin-2, and caveolin-3 (*18*, *23*−*25*). The expression pattern of these isoforms is distinct in different tissues. Caveolin-1 and caveolin-2 are highly coexpressed in adipocytes, endothelial cells, pneumocytes, and fibroblasts, whereas caveolin-3 expression is limited to muscle cells (*22*, *24*). Intriguingly, the expression of all three isoforms of caveolin has been found in only smooth muscle cells as tested so far, with all caveolin isoforms assuming a predominantly plasma membrane distribution (*26*).

Studies suggest that the particular caveolin isoform required for the formation of caveolae invaginations in VSM cells is CAV-1, while CAV-3 drives the expression of caveolae in striated muscle types (cardiac and skeletal) (*22*, *27*). Studies in CAV-1 null mice demonstrated suppression of caveolae in VSM cells, while caveolae formation remained present in striated muscle types (*27*), suggesting that CAV-1 is required for caveolae formation in smooth muscle and that CAV-3 cannot compensate for the physiological function of CAV-1 in smooth muscle cells. Moreover, in CAV-3 null mice, skeletal and heart muscle lack caveolae, whereas smooth muscle still demonstrated formation of caveolae invaginations (*28*). Additionally, CAV-3 expression is completely abolished in CAV-3 null mice, whereas the expression of CAV-1 and CAV-2 is not affected (*28*). The concept that CAV-1 is the caveolin isoform required for caveolae formation in VSM cells highlights the significance of our studies in elucidating the role of CAV-1 in the regulation of VSM metabolism.

Caveolae are organized as oligomers of caveolin proteins in the membrane and create a scaffold on which a variety of molecules are brought together in preassembled complexes (*18*, *22*, *24*, *29*−*31*). Smooth muscle cells contain abundant caveolae that are organized into distinct patches or bands on the cell surface (*32*). Caveolae have been proposed to provide scaffolding for compartmentalized signal transduction, and thus, we proposed that caveolae might provide scaffolding for localization of glycolytic enzymes. Caveolae also have been reported to contain proteins related to glucose metabolism, including PFK (*4*, *16*, *17*), the insulin receptor (*33*−*35*), and GLUT-4 (*36*−*38*). Furthermore, the possibility that PFK may be localized to caveolae is supported by recent data that demonstrate the localization of PFK with CAV-3 in differentiated skeletal myotubes (*16*), the targeting of PFK to the plasma membrane and caveolae fractions in Cos-7 cells after coexpression of both proteins (*17*), and their dynamic regulation by the extracellular glucose concentration and intracellular metabolites in both studies (*16*, *17*). Thus, we proposed that caveolae might provide scaffolding for localization of glycolytic enzymes in VSM. However, there are no studies related to the association of PFK with caveolae in smooth muscle. Therefore, given the previous speculation that CAV-1 is the caveolin isoform required for caveolae formation in VSM cells, we propose that association of CAV-1 with the specific glycolytic enzyme PFK may provide part of the physical basis for compartmentation of glycolysis from related metabolic pathways.

MATERIALS AND METHODS

Cell Culture. A VSM cell line from rat aorta, A7r5 (American Type Culture Collection, Manassas, VA), was grown in 25 cm^2 flasks (Corning, Cambridge, MA) on 13 mm diameter Thermanox coverslips (Electron Microscopy Sciences, Washington, PA), and on 25 mm diameter glass coverslips (Fisherbrand, Pittsburgh, PA) in Dulbecco's modified Eagle's medium (DMEM, Sigma, St. Louis, MO) with added 5.5 mM D-glucose, 26.2 mM Na_2HCO_3, 1 mM sodium pyruvate, and 4 mM L-glutamine. DMEM was supplemented with 10% fetal bovine serum (Gibco, Grand Island, NY) and a 1% antibiotic antimycotic solution (Sigma). Cell propagation was carried out in a 5% CO_2 humidified chamber at 37 °C, and the medium was changed every other day to avoid microbial contamination.

siRNA Transfection in A7r5 Cells. A7r5 cells were transfected with two different sequences of caveolin-1 small interference RNA (CAV-1 siRNA) using a siRNA transfection kit (Silencer siRNA Transfection Kit, Ambion Inc., Austin, TX). The two CAV-1 siRNA sequences that were used (CAV-1-1 siRNA and CAV-1-2 siRNA) were custom designed against the CAV-1 gene sequences 5′AAGGAGATCGACCTGGTCAAC3′ and 5′AAGGGACACACAGTTTTGACG3′ by Ambion Inc. Medium was removed from each coverslip and replaced with 2 mL of CAV-1 siRNA transfection solution composed of 40 μL of siPORT lipid transfection agent, 20 μL of CAV-1-1 siRNA, 20 μL of CAV-1-2 siRNA, and 1.2 mL of Opti-MEM I Reduced Serum Medium (Gibco). Cells were incubated in transfection solution for 6 h in a 5% CO_2 humidified chamber at 37 °C. After transfection medium was replaced with serum-free DMEM supplemented with a 1% (v/v) antibiotic antimycotic solution (Sigma) without siRNA, cells were incubated for 48 h to allow gene downregulation.

Cell Lysate Preparation. Cultured A7r5 cells grown previously in 25 cm^2 flasks and transfected with CAV-1 siRNA (CAV-1-1 and CAV-1-2 siRNA) were transferred to a 15 mL Falcon tube after treatment with trypsin-EDTA (Sigma) and centrifuged at 2600*g* and 25 °C for 5 min. Pelleted cells were resuspended in 200 μL of ice-cold lysis buffer [60 mM octyl glucopyranoside, 1% Triton X-100, 5 mM EDTA, 150 mM NaCl, 1 mM phenylmethanesulfonyl fluoride, and 20 mM Tris (pH 6.4)], transferred to a 1.5 mL centrifuge tube, and incubated for 30 min at 4 °C. Then the cell lysate was sonicated (ELMA Transsonic digital sonicator) for 10 min at maximum power. Finally, the lysate was centrifuged at 15000*g* and 4 °C for 10 min. The supernatant fraction was transferred to a fresh centrifuge tube and stored at −20 °C until SDS−PAGE and Western blot analysis was performed.

SDS−PAGE and Western Blot Analysis. A7r5 cell lysates were separated by SDS−PAGE using a 10% Bis-Tris Criterion XT precast gel (Bio-Rad, Hercules, CA) and then electrotransferred to a 0.2 μm nitrocellulose sheet for Western blot analysis. The protein concentration of each cell lysate was determined by a Bradford assay (Sigma). After being transferred, the nitrocellulose sheets were immunolabeled with rabbit polyclonal caveolin-1 pAb (1:1000) (BD Transduction Laboratories, Lexington, KY) or GAPDH (1:5000) (Silencer siRNA Transfection Kit, Ambion Inc.) followed by alkaline phosphatase-conjugated donkey anti-rabbit IgG

(1:1000) (Rockland Immunochemicals for Research, Gilbertsville, PA) or alkaline phosphatase-conjugated donkey anti-mouse IgG (1:1000) (Rockland Immunochemicals for Research). The nitrocellulose was developed in alkaline phosphatase developing buffer (Bio-Rad) to visualize protein bands. Quantification of the intensity from protein bands was performed by analysis using Image Pro Plus (Media Cybernetics, Silver Spring, MD) after creating a digital scan of the membrane. Areas of interest (AOI) of identical size were created, and the total intensity of the pixels within each protein band was determined using the software. The background intensity of the membrane was subtracted from the value of each AOI to standardize measurements between different membranes. Finally, intensity values from different protein bands were statistically analyzed to determine the percentage difference in intensity.

Electron Microscopy. Cultured A7r5 cells transfected previously with CAV-1 siRNA (CAV-1-1 and CAV-1-2 siRNA) were fixed in the 13 mm Thermonex coverslips in which they were grown with a standard primary fixative (2% glutaraldehyde/2% paraformaldehyde in 0.1 M cacodylate buffer) for 2 h at 25 °C. The primary fixative was followed by three rinses for 15 min each in buffer solution (0.1 M cacodylate buffer) at 25 °C. Then a secondary fixative (1% osmium tetroxide in 0.1 M cacodylate buffer) was used for 2 h at 25 °C followed by three rinses for 15 min each in ultrapure distilled water at 25 °C. Finally, a tertiary fixative (2% uranyl acetate in aqueous solution) was used for 2 h at 25 °C followed by three rinses for 15 min each in ultrapure distilled water at 25 °C. After the fixation process, samples were dehydrated in graded ethanol series of 25, 50, 70, 95, and 100% ethanol for 30 min at 25 °C. The 100% ethanol dehydration step was repeated three more times followed by resin infiltration (Epon Araldite) in a graded resin:ethanol series (1:2, 1:1, and 2:1) and final pure resin for 2 h at 25 °C. Pure resin infiltration was repeated twice more for 4 h each. Finally, embedding capsules were filled with pure resin until a meniscus formed, and the coverslips with specimens were inverted in the top of capsules. The specimens were partially polymerized in a 50−60 °C oven for 24 h. Partially polymerized capsules were submerged in liquid nitrogen for 10 s, and the coverslips were pulled off the capsules, leaving specimens attached to the resin on the capsule. Capsules with specimens were completely polymerized in a 50−60 °C oven for an additional 24 h. Specimens were cut in sections of 70 nm using a LEICA UCT microtome on a diamond knife. Sections were placed on grids and stained in uranyl acetate followed by lead citrate and washed in ultrapure distilled water. Specimens were viewed in a transmission electron microscope at 100000× magnification. All incubation solutions were prepared and provided by the staff of the Electron Microscopy Core at the University of Missouri.

Immunofluorescence Labeling. Cultured A7r5 cells previously transfected with CAV-1 siRNA (CAV-1-1 and CAV-1-2 siRNA) were fixed in the 13 mm coverslips in which they were grown with a paraformaldehyde solution (2% paraformaldehyde, 350 mM NaCl, 160 mM HEPES, and 10 mM $CaCl_2$). Fixed cells were washed with 70% ethanol for 1 min and incubated with 0.2% SUDAN IV (diluted in 70% ethanol) for 30 min to visualize cell membrane boundaries. After 30 min, cells were washed with 70 and 30% ethanol for 1 min each. Then, cells were incubated in a permeabilization solution (50 μM β-escin, 150 mM NaCl, and 15 mM sodium citrate) containing 1% normal donkey serum (Sigma). After the initial permeabilization, cells were incubated overnight in permeabilization solution with 1% normal donkey serum, goat anti-rabbit PFK IgG (1:200) (Rockland Immunochemicals for Research), and mouse monoclonal anti-CAV-1 IgG (1:200) (Research Diagnostics, Inc., Flanders, NJ). After incubation with both primary antibodies, cells were incubated for 3 h in permeabilization solution containing 1% BSA, donkey anti-goat IgG conjugated to Alexa 488 (green) (1:200) (Molecular Probes, Eugene, OR), and donkey anti-mouse IgG conjugated to Alexa 594 (red) (1:200) (Molecular Probes). After incubation with both secondary antibodies, cells were rinsed with a citrate solution containing 150 mM NaCl, 15 mM sodium citrate, and 2% BSA. Finally, coverslips containing immunolabeled cultured cells were placed over glass slides containing Mowiol 4-88 mounting medium. The edges were sealed with a coat of nail enamel to prevent samples from overdrying.

Confocal Microscopy and Image Analysis. Laser scanning confocal microscopy was performed using the Bio-Rad Radiance 2000 instrument (Bio-Rad) on an Olympus IX-70 inverted microscope (Olympus, Tokyo, Japan). Images were captured using a 60× water immersion objective (1.2 UPlan Apo) with a confocal pinhole size of 1.2 um and transmitted to a personal computer with Bio-Rad LaserSharp 2000 (Bio-Rad) and MetaMorph 4.6.9 (Universal Imaging, Chesterfield, PA). All fluorescence images were acquired using the excitation lasers (Bio-Rad) ArKr/Ar 488 (for green) and Kr/Ar 568 (for red) and emission filters (Bio-Rad) of 515 ± 30 nm (for green) and 600 ± 40 nm (for red). All transmitted light images were acquired with Nomarski using a 637 nm red diode laser. Image acquisition was carried out in the *X*, *Y*, and *Z* dimensions with *X*−*Y* resolution of 0.09 μm, *Z* steps of 0.75 μm, and a final image resolution of 1024 × 1024 pixels for all images. The magnification (zoom = 2), laser iris (iris = 1.9 μm), gain, and offset parameters were optimized for each laser (ArKr/Ar 488, Kr/Ar 568, and 637 nm red diode laser) and were kept constant for all images. MetaMorph 4.6.9 was used for image processing after acquisition. For each image, the central *Z* plane was carefully selected. The ratio of overlapping signals from the green fluorescence and red fluorescence images from each sample was reviewed by creating an overlay image. Finally, an analysis of PFK distribution across the cell was performed using the central *Z* plane from each A7r5 sample. Then identical AOIs (30 pixels^2) were created strictly aligned across the entire axis of each cell crossing right next to the nuclear membrane while avoiding pixels inside the nuclei. Each individual AOI was analyzed using the MetaMorph software function for measurement of region statistics. This function displays the dimensional and pixel intensity statistics of the selected region of interest. The average value for pixel intensity within each AOI was determined and plotted as a function of average intensity versus percentage distance across cell. The distribution of PFK throughout the entire cell was further reviewed by creating an intensity profile from the central *Z* plane of each image using MetaMorph. This function creates a topographical profile of the intensity levels within a given image in which "heights" represent brightness in the source image. In addition, a pseudo-color scale was assigned to further distinguish the intensity distributions

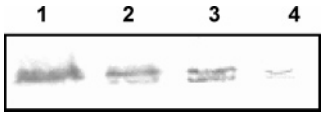

FIGURE 1: Effectiveness of siRNA treatment by targeting of two different sequences within the CAV-1 protein in cultured A7r5 VSM cells. Western blot analysis of A7r5 cells incubated for 6 h with different combinations of two different sequences of siRNAs directed against CAV-1. To test the effectiveness of the siRNA treatment, cells were treated with CAV-1-1 siRNA alone (lane 2), CAV-1-2 siRNA alone (lane 3), and the combination of both CAV-1-1 and CAV-1-2 siRNAs (lane 4). A control group is represented in lane 1. Treatment with both siRNA sequences simultaneously resulted in an ~95% downregulation of CAV-1.

within the profile ranging from black (lowest intensity) to white (highest intensity).

Statistical Analysis. Results are expressed as the mean ± the standard error of the mean of five fields. Statistical significance was determined using a two-tailed paired Student's *t* test assuming unequal variances. *P* values of ≤ 0.05 were considered significant. All statistical calculations were performed using Microsoft Excel 2003.

RESULTS

siRNA Downregulation of CAV-1 mRNA Results in a Reduced Level of Expression of CAV-1 Protein and Inhibition of Caveolae Formation at the Plasma Membrane. To further analyze the role of CAV-1 in metabolic organization, we took advantage of small interference RNA technology (*39*, *40*). We first tested the specificity of the siRNA technology as well as the effectiveness of different transfection agents by studying the downregulation of GAPDH protein levels using a GAPDH siRNA transfection kit designed by Ambion, Inc. Downregulation of GAPDH protein in A7r5 cells was demonstrated to be protein-specific as compared to a scrambled GAPDH siRNA control and to a control group containing all transfection reagents except siRNAs (data not shown). The highest effectiveness was obtained from transfection using the lipid-based transfection agent (data not shown). Once an optimized protocol was identified, we used two different siRNA sequences specifically designed against the CAV-1 mRNA sequence and transfected into cultured A7r5 cells. Control groups of A7r5 cells were treated simultaneously with all transfection reagents except siRNAs. After transfection, cells were placed in serum-free media, which allowed for differentiation into a more contractile phenotype (*41*), and incubated for 48 h to allow CAV-1 downregulation given the half-life of CAV-1 being 20−24 h. After 48 h, cells were analyzed for protein levels and for the presence of caveolae invaginations at the plasma membrane. Transfection of each individual sequence resulted in a 40−50% reduction in CAV-1 protein (Figure 1); however, the combination of both siRNA sequences resulted in an ~95% reduction in the level of CAV-1 protein expression after CAV-1 siRNA transfection as demonstrated by Western blot analysis (Figures 1 and 2A). Downregulation of CAV-1 expression resulted in an apparent decrease in the density of caveolae invaginations at the level of the plasma membrane as evidenced in transmission electron microscopy images as evaluated by visual inspection (Figure 2B). These results demonstrate the effectiveness of the siRNA technology and validate the requirement of the particular CAV-1 protein isoform for the formation of caveolae invaginations in A7r5 VSM cells.

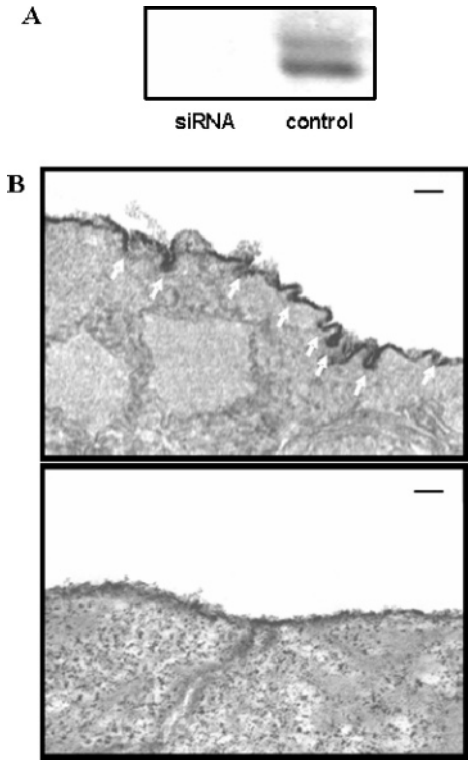

FIGURE 2: siRNA treatment in cultured A7r5 VSM cells results in downregulation of CAV-1 expression and inhibition of caveolae formation at the plasma membrane. Western blot analysis of A7r5 cells incubated for 6 h with two different sequences of siRNAs directed against CAV-1 (A). Cells were then grown for 48 h without siRNA to allow for CAV-1 protein turnover. Electron microscopy demonstrated a reduced level of formation of caveolae invaginations at the level of the plasma membrane in siRNA-treated cells (B, bottom panel) as compared to control A7r5 cells (B, top panel). Control cells are treated with all transfection solutions except siRNAs. The arrows indicate caveolae invaginations in control A7r5 VSM cells. The bar is 100 nm long.

siRNA Transfection Results in a Decreased Level of CAV-1 Expression and a Consequent Shift in the Distribution of PFK with Weaker Localization to the Periphery of the Cells and Increased Immunoreactivity at the Perinuclear Region. To further test the hypothesis that PFK and CAV-1 are co-localized in VSM cells, small interference RNA technology (siRNA) was used to downregulate CAV-1 expression to disrupt the protein−protein interactions between PFK and CAV-1. Confocal microscopy was used to determine the distribution and colocalization of PFK after CAV-1 siRNA downregulation. We observed a significant decrease in the level of immunoreactive CAV-1 as compared to control (Figure 3), validating the decreased protein level measured by Western blot analysis (Figure 2A). We also observed a consequent shift in the distribution of PFK with decreased immunoreactivity of PFK to the periphery of the cells and increased immunoreactivity at the perinuclear region as compared to control (Figure 3), whereas the surface marker SUDAN IV (membrane lipid stain) did not change the location or intensity of PFK (data not shown). The distribution of PFK throughout the entire cell was analyzed by creating an intensity profile from the central *Z* plane of each image using MetaMorph software. Topographical profiles of PFK intensity levels were created using a pseudo-color

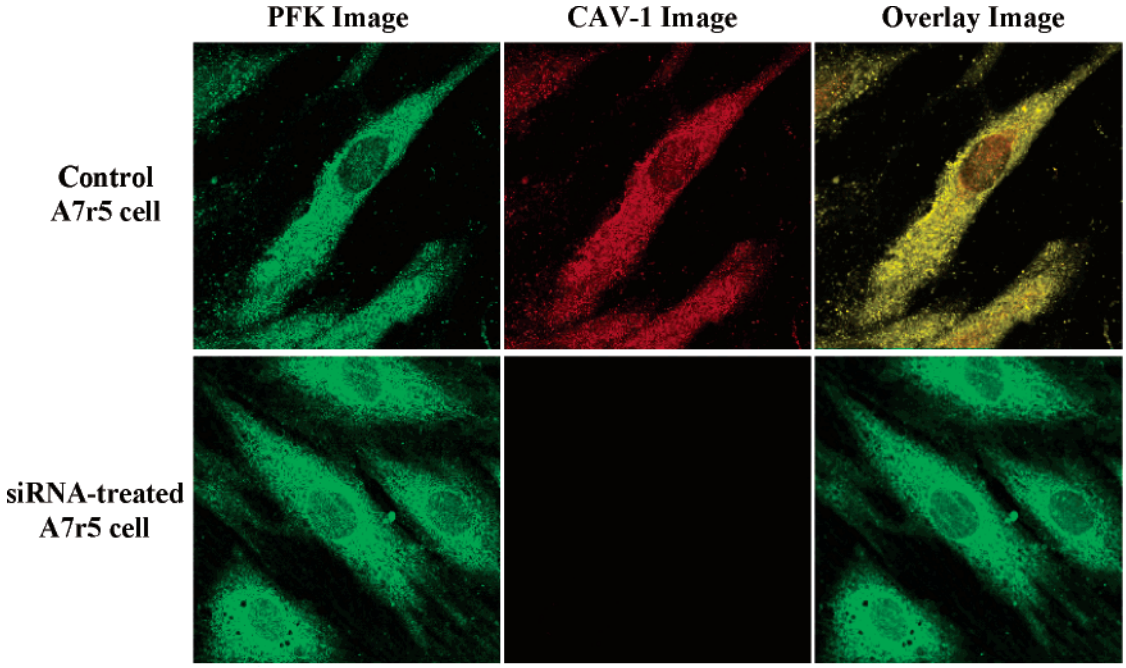

FIGURE 3: siRNA treatment in cultured A7r5 VSM cells results in downregulation of CAV-1 and in redistribution of PFK across cultured rat aorta A7r5 cells. Confocal microscopy images (central *Z* plane) of control and siRNA-treated A7r5 VSM cells immunolabeled for the glycolytic-specific enzyme phosphofructokinase (PFK; Alexa 488 green) and the caveolae-specific protein caveolin-1 (CAV-1; Alexa 594 red). Control cells are treated with all transfection solutions except siRNAs. The overlap between the fluorophores is represented at the right (yellow).

scale ranging from black (lowest intensity) to white (highest intensity) (black < blue < green < yellow < red < white) in which "heights" represent brightness in the source image. The pseudo-color scale in the intensity profile from each image demonstrated decreased PFK intensity at the periphery of the siRNA-treated cells with increased PFK intensity at the perinuclear region as compared to control cells (Figure 4). These results suggest a possible role for CAV-1 as a scaffolding protein for PFK.

Analysis of the Average PFK Intensity across Cultured A7r5 Cells Demonstrates a Higher Central:Peripheral Intensity Ratio (CPI Ratio) in siRNA-Treated Cells Than in the Control. To further analyze the changes in PFK distribution after CAV-1 downregulation, we analyzed the average PFK intensity across cultured A7r5 cells after siRNA treatment. The central *Z* plane from each A7r5 sample was carefully selected, and areas of interest (AOI) of identical size were created across the entire axis of each cell, crossing right next to the nuclear membrane while avoiding pixels inside the nuclei (Figure 5A). Each individual AOI was analyzed for pixel intensity statistics using MetaMorph. The average value for pixel intensity within each AOI was determined and plotted as a function of average intensity versus percentage distance across the cell (Figure 5B). Examples of the distribution of PFK intensity across the cell are plotted in Figure 5B, in which each dotted line represents an individual control A7r5 cell and each solid line represents an individual siRNA-treated A7r5 cell. The analysis from the particular siRNA-treated cell presented in Figure 5A is depicted by the siRNA-1 solid line in the graph in Figure 5B.

There is a clear difference in the shape of the resulting lines from siRNA-treated cells as compared to control cells. siRNA-treated cells clearly exhibit a higher average intensity of PFK toward the center of each line than toward the periphery of each line as compared to the same parameters in control cells. Therefore, the ratio of PFK intensity from the center to the periphery of each line is higher in siRNA-treated cells than in control cells. In an attempt to quantify the difference in PFK intensity from the center to the periphery of each sample, we have developed an equation for determining the central to peripheral intensity ratio (CPI ratio). The CPI ratio for PFK intensity from the total amount of AOIs (even and odd values) across the cells was determined as follows:

$$\text{CPI ratio (even AOI)} = [(m_1 + m_2)/2]/[(p_1 + p_2)/2]$$

$$\text{CPI ratio (odd AOI)} = [(m_1 + m_2 + m_3)/3]/[(p_1 + p_2)/2]$$

in which *m* represents the value for the average PFK intensity from the AOIs in the middle of the axis of each cell while *p* represents the value for the average PFK intensity from the AOIs in the periphery of each cell. The CPI ratio for PFK intensity in siRNA-treated cells (4.6 ± 1.1) was 2.5-fold higher than the CPI ratio for control A7r5 cells (1.8 ± 0.2), indicating a significant ($p = 0.03$) redistribution of PFK after CAV-1 downregulation from the periphery of the cells to the perinuclear area. These results strongly suggest a role for CAV-1 as a scaffolding protein for PFK as evidenced by the redistribution of PFK after CAV-1 downregulation.

DISCUSSION

We have shown that a compartmentation of glycolysis and gluconeogenesis exists in vascular smooth muscle (VSM) cells and that an intact plasma membrane is essential for this compartmentation (*2*−*4*, *8*−*10*). Previously, we observed that disruption of the caveolae inhibited glycolysis but stimulated gluconeogenesis, suggesting a physical link between caveolae and glycolytic enzymes. Using confocal microscopy, we demonstrated a similar distribution of PFK

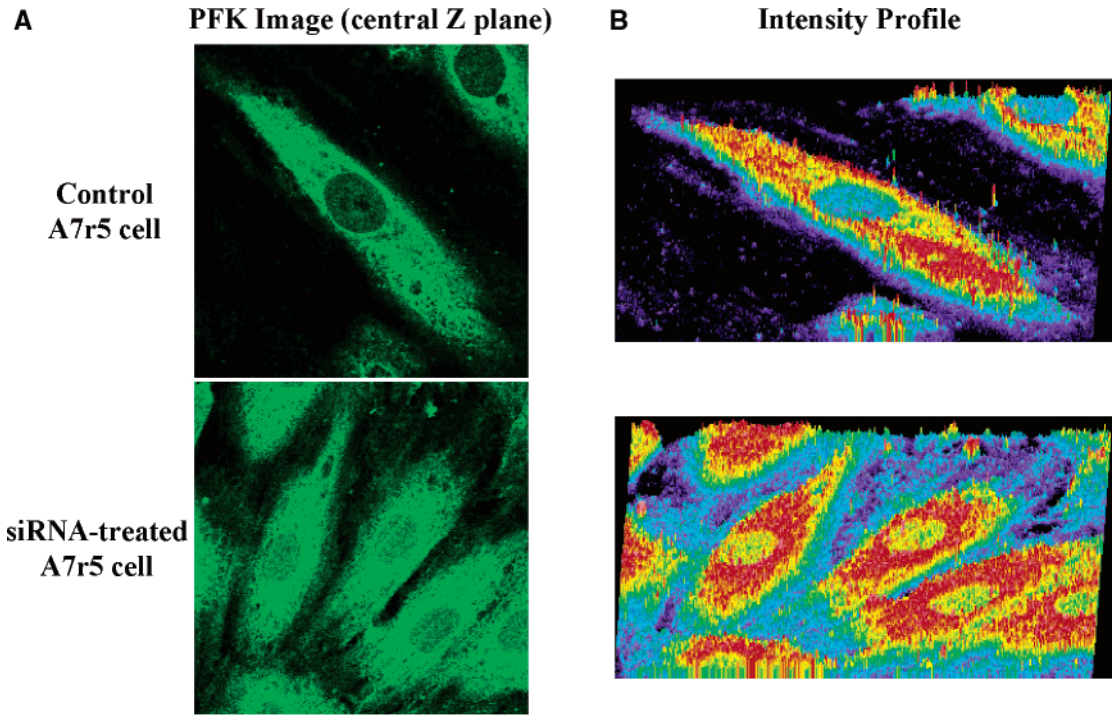

FIGURE 4: Confocal microscopy and profile analysis of PFK redistribution after CAV-1 downregulation in cultured A7r5 VSM cells. The distribution of PFK throughout the entire cell was analyzed by creating an intensity profile from the central *Z* plane of each image using MetaMorph. This function creates a topographical profile of the intensity levels within a given image using a pseudo-color scale ranging from black (lowest intensity) to white (highest intensity) (black < blue < green < yellow < red < white). Profile analysis demonstrated less localization of PFK to the periphery of the siRNA-treated cells with increased immunoreactivity at the perinuclear region compared to control cells. Control cells are treated with all transfection solutions except siRNAs.

with CAV-1 mainly at the periphery (membrane) in freshly isolated VSM cells and in cultured A7r5 cells (*11*). Co-immunoprecipitation analyses validated the interaction between the proteins (*11*). Therefore, the goal of this study was to use siRNA technology to further test the hypothesis that PFK and CAV-1 are colocalized in VSM by downregulation of CAV-1 expression and consequent disruption of the protein−protein interactions between PFK and CAV-1.

In this report, we show that siRNA technology can significantly downregulate the expression of CAV-1 (Figure 2A) and hence the formation of caveolar invaginations at the plasma membrane of cultured A7r5 cells (Figure 2B). Currently, siRNAs are being used extensively in mammalian cells to inhibit expression of specific genes. A critical assumption of this approach is that the siRNA selectively inhibits the complementary gene. However, few groups have encountered nonspecific inhibition of mRNA expression in mammalian cells (*42*). Taking this into account, we used two separate sequences each of 21 bp to prevent the nonspecific inhibition of protein synthesis and RNA degradation observed with sequences longer than 30 bp (*39*). Moreover, we further investigated the specificity of this particular siRNA design technology by studying the downregulation of GAPDH protein levels using both a siRNA sequence against GAPDH and a scramble siRNA with the same base pairs. Only the GAPDH siRNA resulted in GAPDH downregulation, while the scrambled control did cause nonspecific RNA degradation (data not shown). One can argue that this approach tested only the nonspecificity related to the proteins of interest but not to other nonrelated proteins. However, confocal analysis demonstrated that downregulation of the protein of interest (CAV-1) by siRNA transfection resulted in specific protein inhibition without decreasing the total amount of immunoreactive PFK. Therefore, we can assume that the most critical proteins of interest in this study were not affected by the possible nonspecific action of siRNAs. Finally, it is important to note that siRNA technology has been successfully used to downregulate the expression of other proteins in VSM cells recently (*43*, *44*). However, to our knowledge, our study represents the first attempt to use siRNA technology to downregulate CAV-1 expression in VSM.

Downregulation of CAV-1 expression resulted in inhibition of caveolae invaginations at the level of the plasma membrane as evidenced by transmission electron microscopy (Figure 2B). These results validate the effectiveness of the siRNA transfection in these studies. Furthermore, these findings are consistent with studies that suggest that the particular caveolin isoform required for the formation of caveolae invaginations in VSM cells is CAV-1, while CAV-3 drives the expression of caveolae in striated muscle types (cardiac and skeletal) (*22*, *27*). The concept that CAV-1 is the caveolin isoform required for caveolae formation in VSM cells highlights the significance of our studies in elucidating the role of VSM caveolae in the regulation of VSM metabolism.

siRNA transfection resulted in a decreased level of CAV-1 expression and a shift in the distribution of PFK with less localization to the periphery of the cells and increased immunoreactivity at the perinuclear region as demonstrated by the PFK intensity profiles (Figure 4). Analysis of the average PFK intensity across cultured A7r5 cells demonstrated a higher central to peripheral intensity ratio (CPI ratio) in siRNA-treated cells than in the control (Figure 5B). These results suggest a massive mobilization of PFK from the

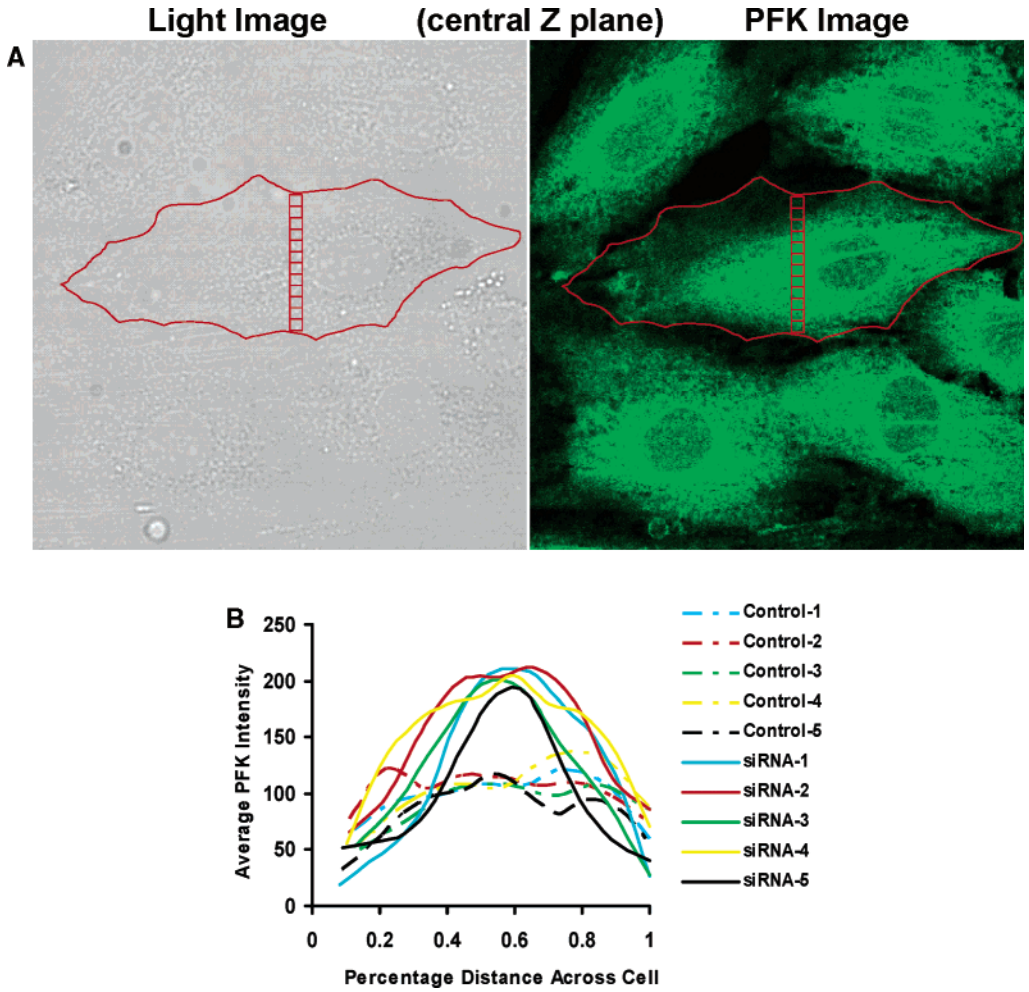

FIGURE 5: Analysis of the average PFK intensity across cultured A7r5 cells after CAV-1 downregulation by siRNA treatment. The central *Z* plane from each A7r5 sample was carefully selected, and identical areas of interest (AOI) were created across the entire axis of each cell, crossing right next to the nuclear membrane (A). Each individual AOI was analyzed for pixel intensity statistics, and the average value for pixel intensity was determined and plotted as a function of average intensity vs the percentage distance across the cell (B). The analysis for the representative sample (A) is represented by the bold line identified as siRNA-1 (B). siRNA transfection resulted in a decreased level of CAV-1 expression and a consequent shift in the distribution of PFK with less localization to the periphery of the cells and increased immunoreactivity at the perinuclear region. Control cells are treated with all transfection solutions except siRNAs.

plasma membrane to the perinuclear membranes and other cytoskeletal locations after CAV-1 downregulation, indicating that CAV-1 plays a role in the localization of PFK to the plasma membrane. The localization of PFK to other cytoplasmic locations is consistent with considerable evidence that suggests that glycolytic enzymes not only are found in association with the plasma membrane (*4*, *42*, *45*−*48*) but also may be in association with the microtubules (*12*, *49*−*54*) and F-actin (*55*−*57*), resulting in different glycolytic cascades associated with different cellular domains. Moreover, studies in skeletal muscle from wild-type mice have found that PFK localizes to the sarcolemma (plasma membrane) as well as intracellularly, whereas in CAV-3 deficient mice, PFK is localized to cytoplasmic regions and not targeted to the sarcolemma or to caveolae-enriched microdomains (*17*). These studies provide an interesting parallel to our results in PFK distribution after CAV-1 downregulation in VSM. However, our studies are novel since they emphasized a different caveolin isoform in a unique system in caveolae biology as VSM represents the only cell type with coexpression of all caveolin isoforms and the only muscle type in which caveolae biogenesis is driven by CAV-1 instead of CAV-3.

It is important to highlight that our previous studies used confocal microscopy to determine the distribution and colocalization of PFK and CAV-1 in both freshly isolated VSM and cultured VSM cells (*11*). We observed that CAV-1 largely exhibited peripheral (membrane) localization in freshly isolated cells with some CAV-1 fluorescence also observed at intracellular loci. However, in cultured A7r5 cells, CAV-1 localization was observed at intracellular loci with significantly less peripheral localization (*11*). These results suggested that the CPI ratio of PFK intensity could be even more significant if evaluated in freshly isolated VSM cells as compared to siRNA-treated A7r5 cells. Therefore, we proceeded to carry out the analysis from previous data and found that the CPI ratio in freshly isolated VSM cells was 0.4 ± 0.1, which indicates a higher PFK intensity at the periphery of the cells than in the intracellular areas as compared to control A7r5 cells (CPI ratio $= 1.8 \pm 0.2$) and siRNA-treated A7r5 cells (CPI ratio $= 4.6 \pm 1.1$). This analysis supports our previous results and suggests that CAV-1 downregulation in freshly isolated cells could potentially result in a more dramatic redistribution of PFK after siRNA transfection.

Taken together, these results validate the possible role of CAV-1 as a scaffolding protein for PFK *in vivo* as evidenced by changes in the CPI ratio of PFK intensity and the redistribution of PFK after CAV-1 downregulation. Moreover, our studies are consistent with studies that have demonstrated that CAV-1 co-immunoprecipitates with PFK-M from 293T cells transiently overexpressing V5-tagged PFK-M (*17*). The same studies also demonstrated that recombinant expression of CAV-1 in Cos-7 cells induces membrane targeting of overexpressed V5-tagged PFK-M (*17*). However, it is important to highlight that these studies were performed by analysis of the interaction between recombinant expression of both PFK and CAV-1 proteins instead of endogenous proteins (*17*). Our studies are novel in the fact that we are analyzing the interaction of endogenous proteins in VSM.

Although our results clearly demonstrate a role of CAV-1 as a scaffolding protein for PFK, at normal levels of CAV-1 (control A7r5 cells) there is a substantial fraction of PFK not colocalized with CAV-1. This suggests either that there is not sufficient CAV-1 in the cell to interact with all the PFK or that CAV-1 is only one of multiple scaffolding proteins that compete for PFK binding and localization. Experiments similar to the ones performed here but targeting other putative glycolytic enzyme scaffolding proteins (such as tubulin and actin) should be performed to evaluate the relative glycolytic enzyme binding affinities and hence the relative roles in glycolytic enzyme localization and organization.

The demonstration that CAV-1 functions as a scaffolding protein for the membrane recruitment of PFK in VSM cells is a very important step in elucidating the role of caveolae in the organization of carbohydrate metabolism and in defining the pathogenic mechanisms underlying diseases that involved alterations in cellular metabolism. Previous studies have demonstrated a parallel role for CAV-3 and PFK in the pathogenesis of CAV-3-related muscle diseases such as limb-girdle muscular dystrophy-1C, distal myopathy, and rippling muscle disease that are caused by mutations within the human CAV-3 gene (*17*). However, no studies have defined the role of CAV-1 and PFK in cellular metabolism. We hypothesized that PFK might be recruited to the caveolae membrane domain of VSM cells by interaction with CAV-1, which allows them to be close to a variety of proteins related to glucose metabolism. For example, the insulin receptor, which regulates glucose uptake, has been found to interact with CAV-1 (*33*−*35*). GLUT-4, the insulin-responsive glucose transporter, has been localized to caveolae in skeletal muscle (*37*), and adipocytes (*36*, *38*); therefore, GLUT-1 might have a similar localization in VSM.

The concept that CAV-1 coordinates the subcellular distribution of the key player of the glycolytic pathway, namely, PFK, highlights the important role of caveolae in the regulation of energy metabolism in VSM cells by allowing a more rapid and efficient control of glucose metabolism through the compartmentation of PFK, GLUT-1, and the insulin receptor to the caveolae membrane domain. Taken together, we conclude that CAV-1 functions as a scaffolding protein for PFK and that this contributes to the compartmentation of glycolysis from other metabolic pathways in VSM, allowing for a more efficient control of glucose metabolism and providing localized energetic support of kinases and other membrane proteins within the caveolae.

ACKNOWLEDGMENT

We thank Dr. Mayandi Sivaguru for assistance with the confocal microscopy (Molecular Cytology Core, University of Missouri). We also thank Randy Tindal and Cheryl Jensen for advice and assistance with transmission electron microscopy (Electron Microscopy Core, University of Missouri). The assistance of Tina Roberts is greatly appreciated.

REFERENCES

1. Bouzier, A. K., Goodwin, R., de Gannes, F. M., Valeins, H., Voisin, P., Canioni, P., and Merle, M. (1998) Compartmentation of lactate and glucose metabolism in C6 glioma cells. A ^{13}C and ^{1}H NMR study, *J. Biol. Chem. 273*, 27162−27169.
2. Lloyd, P. G., and Hardin, C. D. (1999) Role of microtubules in the regulation of metabolism in isolated cerebral microvessels, *Am. J. Physiol. 277*, C1250−C1262.
3. Lloyd, P. G., and Hardin, C. D. (2000) Sorting of metabolic pathway flux by the plasma membrane in cerebrovascular smooth muscle cells, *Am. J. Physiol. 278*, C803−C811.
4. Lloyd, P. G., and Hardin, C. D. (2001) Caveolae and the organization of carbohydrate metabolism in vascular smooth muscle, *J. Cell. Biochem. 82*, 399−408.
5. Damico, L. A., White, L. T., Yu, X., and Lewandowski, E. D. (1996) Chemical versus isotopic equilibrium and the metabolic fate of glycolytic end products in the heart, *J. Mol. Cell. Cardiol. 28*, 989−999.
6. Lewandowski, E. D. (1992) Metabolic heterogeneity of carbon substrate utilization in mammalian heart: NMR determinations of mitochondrial versus cytosolic compartmentation, *Biochemistry 31*, 8916−8923.
7. Zwingmann, C., Richter-Landsberg, C., and Leibfritz, D. (2001) ^{13}C isotopomer analysis of glucose and alanine metabolism reveals cytosolic pyruvate compartmentation as part of energy metabolism in astrocytes, *Glia 34*, 200−212.
8. Hardin, C. D., Allen, T. J., and Paul, R. J. (2001) in *Heart Physiology and Pathophysiology*, pp 579−583, Academic Press, New York.
9. Hardin, C. D., and Roberts, T. M. (1995) Compartmentation of glucose and fructose 1,6-bisphosphate metabolism in vascular smooth muscle, *Biochemistry 34*, 1323−1331.
10. Hardin, C. D., and Finder, D. R. (1998) Glycolytic flux in permeabilized freshly isolated vascular smooth muscle cells, *Am. J. Physiol. 274*, C88−C96.
11. Vallejo, J., and Hardin, C. D. (2004) Metabolic organization in vascular smooth muscle: Distribution and localization of caveolin-1 and phosphofructokinase, *Am. J. Physiol. 286*, C43−C54.
12. Lehotzky, A., Telegdi, M., Liliom, K., and Ovadi, J. (1993) Interaction of phosphofructokinase with tubulin and microtubules. Quantitative evaluation of the mutual effects, *J. Biol. Chem. 268*, 10888−10894.
13. Hazen, S. L., and Gross, R. W. (1993) The specific association of a phosphofructokinase isoform with myocardial calcium-independent phospholipase A2. Implications for the coordinated regulation of phospholipolysis and glycolysis, *J. Biol. Chem. 268*, 9892−9900.
14. Chen-Zion, M., Bassukevitz, Y., and Beitner, R. (1992) Sequence of insulin effects on cytoskeletal and cytosolic phosphofructokinase, mitochondrial hexokinase, glucose 1,6-bisphosphate and fructose 2,6-bisphosphate levels, and the antagonistic action of calmodulin inhibitors, in diaphragm muscle, *Int. J. Biochem. 24*, 1661−1667.
15. Firestein, B. L., and Bredt, D. S. (1999) Interaction of neuronal nitric-oxide synthase and phosphofructokinase-M, *J. Biol. Chem. 274*, 10545−10550.
16. Scherer, P. E., and Lisanti, M. P. (1997) Association of phosphofructokinase-M with caveolin-3 in differentiated skeletal myotubes. Dynamic regulation by extracellular glucose and intracellular metabolites, *J. Biol. Chem. 272*, 20698−20705.
17. Sotgia, F., Bonuccelli, G., Minetti, C., Woodman, S. E., Capozza, F., Kemp, R. G., Scherer, P. E., and Lisanti, M. P. (2003) Phosphofructokinase muscle-specific isoform requires caveolin-3 expression for plasma membrane recruitment and caveolar targeting: Implications for the pathogenesis of caveolin-related muscle diseases, *Am. J. Pathol. 163*, 2619−2634.

18. Anderson, R. G. (1998) The caveolae membrane system, *Annu. Rev. Biochem. 67*, 199−225.
19. Luetterforst, R., Stang, E., Zorzi, N., Carozzi, A., Way, M., and Parton, R. G. (1999) Molecular characterization of caveolin association with the Golgi complex: Identification of a cis-Golgi targeting domain in the caveolin molecule, *J. Cell Biol. 145*, 1443−1459.
20. Thyberg, J. (2000) Differences in caveolae dynamics in vascular smooth muscle cells of different phenotypes, *Lab. Invest. 80*, 915−929.
21. Machleidt, T., Li, W. P., Liu, P., and Anderson, R. G. (2000) Multiple domains in caveolin-1 control its intracellular traffic, *J. Cell Biol. 148*, 17−28.
22. Razani, B., Woodman, S. E., and Lisanti, M. P. (2002) Caveolae: From cell biology to animal physiology, *Pharmacol. Rev. 54*, 431−467.
23. Smart, E. J., Graf, G. A., McNiven, M. A., Sessa, W. C., Engelman, J. A., Scherer, P. E., Okamoto, T., and Lisanti, M. P. (1999) Caveolins, liquid-ordered domains, and signal transduction, *Mol. Cell. Biol. 19*, 7289−7304.
24. Schlegel, A., and Lisanti, M. P. (2001) Caveolae and their coat proteins, the caveolins: From electron microscopic novelty to biological launching pad, *J. Cell. Physiol. 186*, 329−337.
25. Engelman, J. A., Zhang, X. L., Galbiati, F., and Lisanti, M. P. (1998) Chromosomal localization, genomic organization, and developmental expression of the murine caveolin gene family (Cav-1, -2, and -3). Cav-1 and Cav-2 genes map to a known tumor suppressor locus (6-A2/7q31), *FEBS Lett. 429*, 330−336.
26. Taggart, M. J. (2001) Smooth muscle excitation-contraction coupling: A role for caveolae and caveolins? *News Physiol. Sci. 16*, 61−65.
27. Razani, B., and Lisanti, M. P. (2001) Caveolin-deficient mice: Insights into caveolar function human disease, *J. Clin. Invest. 108*, 1553−1561.
28. Galbiati, F., Engelman, J. A., Volonte, D., Zhang, X. L., Minetti, C., Li, M., Hou, H., Jr., Kneitz, B., Edelmann, W., and Lisanti, M. P. (2001) Caveolin-3 null mice show a loss of caveolae, changes in the microdomain distribution of the dystrophin-glycoprotein complex, and t-tubule abnormalities, *J. Biol. Chem. 276*, 21425−21433.
29. Okamoto, T., Schlegel, A., Scherer, P. E., and Lisanti, M. P. (1998) Caveolins, a family of scaffolding proteins for organizing "pre-assembled signaling complexes" at the plasma membrane, *J. Biol. Chem. 273*, 5419−5422.
30. Couet, J., Li, S., Okamoto, T., Ikezu, T., and Lisanti, M. P. (1997) Identification of peptide and protein ligands for the caveolin-scaffolding domain. Implications for the interaction of caveolin with caveolae-associated proteins, *J. Biol. Chem. 272*, 6525−6533.
31. Liu, P., Rudick, M., and Anderson, R. G. (2002) Multiple functions of caveolin-1, *J. Biol. Chem. 277*, 41295−41298.
32. Severs, N. J., and Simons, H. L. (1986) Caveolar bands and the effects of sterol-binding agents in vascular smooth muscle plasma membrane. Single and double labeling with filipin and tomatin in the aorta, pulmonary artery, and vena cava, *Lab. Invest. 55*, 295−307.
33. Kimura, A., Mora, S., Shigematsu, S., Pessin, J. E., and Saltiel, A. R. (2002) The insulin receptor catalyzes the tyrosine phosphorylation of caveolin-1, *J. Biol. Chem. 277*, 30153−30158 [erratum: (2002) *J. Biol. Chem. 277*, 40167].
34. Parpal, S., Karlsson, M., Thorn, H., and Stralfors, P. (2001) Cholesterol depletion disrupts caveolae and insulin receptor signaling for metabolic control via insulin receptor substrate-1, but not for mitogen-activated protein kinase control, *J. Biol. Chem. 276*, 9670−9678.
35. Yamamoto, M., Toya, Y., Schwencke, C., Lisanti, M. P., Myers, M. G., Jr., and Ishikawa, Y. (1998) Caveolin is an activator of insulin receptor signaling, *J. Biol. Chem. 273*, 26962−26968.
36. Karlsson, M., Thorn, H., Parpal, S., Stralfors, P., and Gustavsson, J. (2002) Insulin induces translocation of glucose transporter GLUT4 to plasma membrane caveolae in adipocytes, *FASEB J. 16*, 249−251.
37. Friedman, J. E., Dudek, R. W., Whitehead, D. S., Downes, D. L., Frisell, W. R., Caro, J. F., and Dohm, G. L. (1991) Immunolocalization of glucose transporter GLUT4 within human skeletal muscle, *Diabetes 40*, 150−154.
38. Scherer, P. E., Lisanti, M. P., Baldini, G., Sargiacomo, M., Mastick, C. C., and Lodish, H. F. (1994) Induction of caveolin during adipogenesis and association of GLUT4 with caveolin-rich vesicles, *J. Cell Biol. 127*, 1233−1243.
39. Elbashir, S. M., Harborth, J., Lendeckel, W., Yalcin, A., Weber, K., and Tuschl, T. (2001) Duplexes of 21-nucleotide RNAs mediate RNA interference in cultured mammalian cells, *Nature 411*, 494−498.
40. Persengiev, S. P., Zhu, X., and Green, M. R. (2004) Nonspecific, concentration-dependent stimulation and repression of mammalian gene expression by small interfering RNAs (siRNAs), *RNA 10*, 12−18.
41. Thyberg, J. (1996) Differentiated properties and proliferation of arterial smooth muscle cells in culture, *Int. Rev. Cytol. 169*, 183−265.
42. Green, D. E., Murer, E., Hultin, H. O., Richardson, S. H., Salmon, B., Brierley, G. P., and Baum, H. (1965) Association of integrated metabolic pathways with membranes. I. Glycolytic enzymes of the red blood corpuscle and yeast, *Arch. Biochem. Biophys. 112*, 635−647.
43. Li, Y., Lu, W., and Bu, G. (2003) Essential role of the low-density lipoprotein receptor-related protein in vascular smooth muscle cell migration, *FEBS Lett. 555*, 346−350.
44. Kloss, S., Furneaux, H., and Mulsch, A. (2003) Post-transcriptional regulation of soluble guanylyl cyclase expression in rat aorta, *J. Biol. Chem. 278*, 2377−2383.
45. Hardin, C. D., Raeymaekers, L., and Paul, R. J. (1992) Comparison of endogenous and exogenous sources of ATP in fueling Ca^{2+} uptake in smooth muscle plasma membrane vesicles, *J. Gen. Physiol. 99*, 21−40.
46. Dizon, J., Burkhoff, D., Tauskela, J., Whang, J., Cannon, P., and Katz, J. (1998) Metabolic inhibition in the perfused rat heart: Evidence for glycolytic requirement for normal sodium homeostasis, *Am. J. Physiol. 274*, H1082−H1089.
47. Paul, R. J., Bauer, M., and Pease, W. (1979) Vascular smooth muscle: Aerobic glycolysis linked to sodium and potassium transport processes, *Science 206*, 1414−1416.
48. Paul, R. J., Hardin, C. D., Raeymaekers, L., Wuytack, F., and Casteels, R. (1989) Preferential support of Ca^{2+} uptake in smooth muscle plasma membrane vesicles by an endogenous glycolytic cascade, *FASEB J. 3*, 2298−2301.
49. Vertessy, B. G., Orosz, F., Kovacs, J., and Ovadi, J. (1997) Alternative binding of two sequential glycolytic enzymes to microtubules. Molecular studies in the phosphofructokinase/aldolase/microtubule system, *J. Biol. Chem. 272*, 25542−25546.
50. Vertessy, B. G., Kovacs, J., Low, P., Lehotzky, A., Molnar, A., Orosz, F., and Ovadi, J. (1997) Characterization of microtubule-phosphofructokinase complex: Specific effects of MgATP and vinblastine, *Biochemistry 36*, 2051−2062.
51. Lehotzky, A., Palfia, Z., Kovacs, J., Molnar, A., and Ovadi, J. (1994) Ligand-modulated cross-bridging of microtubules by phosphofructokinase, *Biochem. Biophys. Res. Commun. 204*, 585−591.
52. Schwartz, D., and Beitner, R. (2000) Detachment of the glycolytic enzymes, phosphofructokinase and aldolase, from cytoskeleton of melanoma cells, induced by local anesthetics, *Mol. Genet. Metab. 69*, 159−164.
53. Glass-Marmor, L., and Beitner, R. (1999) Taxol (paclitaxel) induces a detachment of phosphofructokinase from cytoskeleton of melanoma cells and decreases the levels of glucose 1,6-bisphosphate, fructose 1,6-bisphosphate and ATP, *Eur. J. Pharmacol. 370*, 195−199.
54. Karkhoff-Schweizer, R., and Knull, H. R. (1987) Demonstration of tubulin-glycolytic enzyme interactions using a novel electrophoretic approach, *Biochem. Biophys. Res. Commun. 146*, 827−831.
55. Kao, A. W., Noda, Y., Johnson, J. H., Pessin, J. E., and Saltiel, A. R. (1999) Aldolase mediates the association of F-actin with the insulin-responsive glucose transporter GLUT4, *J. Biol. Chem. 274*, 17742−17747.
56. Bronstein, W. W., and Knull, H. R. (1981) Interaction of muscle glycolytic enzymes with thin filament proteins, *Can. J. Biochem. 59*, 494−499.
57. Knull, H. R., Bronstein, W. W., DesJardins, P., and Niehaus, W. G. (1980) Interaction of selected brain glycolytic enzymes with an F-actin-tropomyosin complex, *J. Neurochem. 34*, 222−225.

BI0490035